Available online at www.sciencedirect.com
ScienceDirect
Journal of Power Sources 171 (2007) 626–633
JOURNAL OF POWER SOURCES
www.elsevier.com/locate/jpowsour

Voltage instability in a simulated fuel cell stack correlated to cathode water accumulation

J.P. Owejan [a,*], T.A. Trabold [a], J.J. Gagliardo [a], D.L. Jacobson [b], R.N. Carter [a], D.S. Hussey [b], M. Arif [b]

[a] *General Motors Fuel Cell Activities, 10 Carriage Street, Honeoye Falls, NY 14472-0603, USA*
[b] *National Institute of Standards and Technology (NIST), Center for Neutron Research, 100 Bureau Drive, M.S 8461, Gaithersburg, MD 20899-8461, USA*

Received 20 April 2007; received in revised form 15 June 2007; accepted 19 June 2007
Available online 22 July 2007

Abstract

Single fuel cells running independently are often used for fundamental studies of water transport. It is also necessary to assess the dynamic behavior of fuel cell stacks comprised of multiple cells arranged in series, thus providing many paths for flow of reactant hydrogen on the anode and air (or pure oxygen) on the cathode. In the current work, the flow behavior of a fuel cell stack is simulated by using a single-cell test fixture coupled with a bypass flow loop for the cathode flow. This bypass simulates the presence of additional cells in a stack and provides an alternate path for airflow, thus avoiding forced convective purging of cathode flow channels. Liquid water accumulation in the cathode is shown to occur in two modes; initially nearly all the product water is retained in the gas diffusion layer until a critical saturation fraction is reached and then water accumulation in the flow channels begins. Flow redistribution and fuel cell performance loss result from channel slug formation. The application of *in-situ* neutron radiography affords a transient correlation of performance loss to liquid water accumulation. The current results identify a mechanism whereby depleted cathode flow on a single cell leads to performance loss, which can ultimately cause an operating proton exchange membrane fuel cell stack to fail.

Keywords: PEMFC; Water transport; Diagnostics; Neutron imaging; Gas diffusion layer; Flow channel

1. Introduction

Proton exchange membrane fuel cell (PEMFC) technology is being actively developed for portable, stationary and automotive applications. This technology is of particular interest as an economically viable replacement for the internal combustion engine that would reduce greenhouse emissions and petroleum consumption. An important area of PEMFC research is the transport of the water produced during the oxygen reduction reaction at the cathode electrode. Due to the slow kinetics associated with oxygen reduction in the cathode relative to hydrogen oxidation in the anode, as well as water generation in the cathode, mass transfer to and from the cathode electrode represents the primary fundamental limitation to fuel cell operation. An efficient fuel cell stack design requires a comprehensive understanding of liquid phase water transport throughout the cathode volume.

There is a significant amount of published research focused on the development and application of diagnostic techniques to interrogate operating fuel cells for liquid water formation and dynamics [1–4]. Among these techniques, neutron imaging of an operating single cell [5–10] is the most robust because minimal modifications to the fuel cell are required to generate quantitative two-dimensional liquid water distributions. Most fundamental fuel cell experiments employ only one cell instead of the stack of cells that is required for high voltage operation. There are several advantages to single-cell experiments, including more accurate control of pressure, stoichiometric ratios and electric load. A primary driver for single-cell experiments is also cost as test systems and materials for a PEMFC stacks are very expensive in the current state of the technology. Also, a single cell allows unambiguous interpretation of neutron radiography images, whereas a multi-cell stack would complicate this anal-

* Corresponding author. Tel.: +1 585 624 6802; fax: +1 585 624 6680.
E-mail address: jon.owejan@gm.com (J.P. Owejan).

0378-7753/$ – see front matter © 2007 Elsevier B.V. All rights reserved.
doi:10.1016/j.jpowsour.2007.06.174

Nomenclature

GDL	gas diffusion layer
MEA	membrane electrode assembly
t	time (s)
$V_{GDL,crit}$	critical water volume for GDL (cm^3)
$V_{GDL,open}$	open pore volume for GDL (cm^3)
V_w	water volume (cm^3)
V_{wo}	reference (initial) water volume (cm^3)

Greek letter

ζ	stoichiometric ratio

ysis. However, a stack experiment is of particular interest for liquid water transport studies. It is known that the additional flow paths provided by many bipolar plates connected to a common manifold can result in localized liquid water accumulation in the gas delivery channels of one cell becoming severe relative to the rest of the cells in a stack [11,12]. This liquid accumulation mechanism results from plate pressure drop variations due to dimensional differences in channel geometry from machining deviations or gas diffusion layer (GDL) intrusion into channel cross-section. Given the flow dynamics of a stack, the disadvantage of a liquid water transport visualization experiment with one cell is obvious because all the inlet flow must travel into a single flow distributor. Flow field blockages will be reduced with a single-cell experiment as the pressure increase will eliminate liquid water obstructions. This fails to demonstrate a situation that can easily be imagined in a stack of hundreds of cells, where one blocked cell has an immeasurable effect on the overall system pressure drop. This PEMFC stack cell blockage scenario is believed to cause the electrical potential to approach zero as its oxygen flow rate falls below what is required by reaction stoichiometry to sustain the current load. In a large active area system, oxygen diffusion from the manifolds into the stagnant channels is much too slow to sustain the reaction at any practical load.

No diagnostic method currently exists to probe for liquid water content of an individual cell in a PEMFC stack. Although neutron radiography can be applied to an operating stack, the two-dimensional information thus produced would be insufficient for correlating the instability in an individual cell to local liquid water content in the through-plane direction. Also, such an experiment would result in poor image quality due to geometric unsharpness and low-neutron transmission. Three-dimensional tomography techniques may be applied, but are unfavorable as they will not provide enough geometric or temporal resolution for a typical PEMFC stack experiment.

The fuel cell stack failure mechanism described above was investigated in the current study. The experiments were conducted on a single cell with a modified cathode gas delivery system. This system provided a bypass of inlet air around the single-cell cathode flow distributor as inlet pressure increased due to liquid water blockage inside the flow field of the active cell. This system simulates a PEMFC stack by providing an alternative path with nearly the same pressure differential as a dry flow field. The bypass method allows one to consider a realistic liquid water distribution that would occur in a single cell of a typical PEMFC stack and elucidates a stack failure mechanism not captured by fundamental single-cell experiments.

2. Experimental

Experiments were conducted at the National Institute of Standards and Technology (NIST) Center for Neutron Research (CNR) thermal neutron imaging beam [13] with a 50 cm^2 active area PEMFC single-cell test section. The experimental apparatus consisted of a small-scale fuel cell controller and a pressure controlled cathode bypass system. Experiments were conducted at low power (0.2 A cm^{-2}) where the air velocity in cathode channels at the most efficient stoichiometric ratios (input gas flow/required reaction gas flow) nearest to 1.0 is most likely insufficient to convectively force water slugs out of the system. With the PEMFC dry (prior to operation), the bypass system pressure differential was adjusted such that the cathode of the single cell would receive a stoichiometric ratio of 3.4 (maximum flow available with current test equipment) from the supply flow, which was equivalent to that required for a 20 cell stack operating at 0.2 A cm^{-2}.

2.1. Neutron imaging procedure

The neutron imaging procedure, calibration, and data reduction procedure were executed as presented in [9,10]. The liquid water content in the operating fuel cell is described quantitatively by Beer's law, where attenuation contributions of the fuel cell structure are normalized by referencing the fuel cell in the dry state at the average operating temperature. Later, once the fuel cell is operating, the content of liquid water produced from the oxygen reduction reaction is accurately determined from the known macroscopic neutron cross-section for liquid water [10].

2.2. PEMFC test section

The 50 cm^2 hardware used in the current experiments was designed such that liquid water in anode and cathode channels could easily be distinguished. A three-pass serpentine pattern was utilized to maintain reasonable pressure differential within the channels. These flow fields were machined into 1.27 cm thick 6061 aluminum plates then gold plated with a nickel intermediate layer. Aluminum was used for this application for its transparency to neutrons, thus increasing the signal-to-noise ratio needed for short exposure neutron imaging. The nominal dimensions of the anode and cathode channels were 0.5 mm wide and 0.3 mm deep. The flow field channel patterns for both anode and cathode, superimposed as in assembly, are shown in Fig. 1. The anode and cathode flow field patterns are unique with respect to channel overlap while the overall flow direction and performance is maintained. These flow fields allow the discrimination of liquid water on either side of the fuel cell when evaluating the reduced neutron image data.

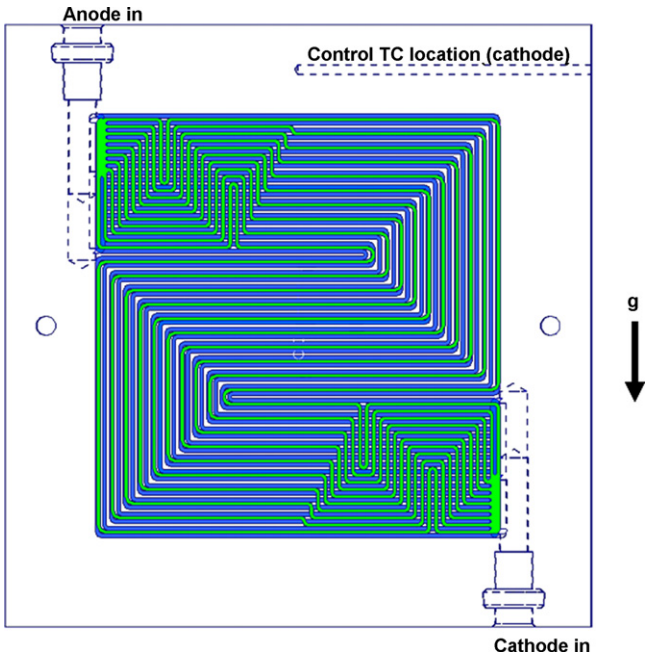

Fig. 1. Anode and cathode flow fields superimposed (anode green, cathode blue). (For interpretation of the references to color in this figure legend, the reader is referred to the web version of the article.)

The single PEMFC was built with SGL Carbon 21BC GDLs and W.L. Gore 18 μm membrane with Pt areal density of 0.4 mg cm^{-2} catalyst loading on the anode and cathode electrodes [14]. The gasket thickness was selected to ensure 20% compressive strain on the GDL substrate. Anode hydrogen gas flow was run counter to cathode air gas flow throughout the experiment, as shown in Fig. 1.

2.3. Simulated stack with cathode bypass

Single-cell PEMFC experiments cannot simulate the possible cell-to-cell flow variation inherent in a fuel cell stack. In a stack of many flow fields, each will receive a slightly different amount of gas flow depending on the dry pressure drop of each cell relative to that of the overall stack. In practice, this effect is minimized by controlling variation between plates. However, liquid water accumulation in an operating stack can exaggerate this effect. The present work is focused on describing this mechanism with a single-cell apparatus that is supplied with stack equivalent airflow where the majority of the flow is allowed to bypass the cell. In this configuration, as the cathode flow field accumulates liquid water and the pressure differential rises, more gas will flow through the bypass leg held at a constant pressure drop. The bypass stack simulation is implemented on the cathode side only, as the majority of product water generated by the PEMFC reaction is managed in the cathode gas delivery system. This is shown experimentally by the relative water removal with a purge of equal volumetric gas flow applied to the anode and cathode individually.

The bypass mechanization process flow diagram is shown in Fig. 2. The system allows the simulation of cathode flow distribution in a stack of 20 cells with an active area of 50 cm^2 while operating just a single-test cell. The bypass pressure differential is set equal to that of the test cell when the cell is known to be in a dry reference state. The cathode stoichiometric ratio is monitored with two separate measurements. The first is a calibrated mass flow meter and the second is an oxygen sensor that measured fraction of oxygen concentration in the outlet stream. Each of these, combined with the known current density, allows one to calculate and monitor the change in cathode stoichiometric ratio as a function of liquid water content (as measured with neutron radiography). The agreement between these two measurement methods was excellent, with an average difference in computed cathode stoichiometric ratio of 2% at steady state.

Experiments were executed by establishing a precondition with the bypass system pressure differential being adjusted to provide a constant cathode stoichiometric ratio through the cell. This precondition was at 0.2 A cm^{-2} with anode and cathode inlet relative humidities of 50 and 65%, respectively, and the system outlet pressure controlled to 114 kPa. The anode and cathode stoichiometric ratios during the precondition were 2.0 and 3.4, respectively. The cell temperature was kept constant at 77 °C throughout the experiment. Once the liquid water content of the cell was determined to be constant with online image analysis, the bypass system was no longer adjusted, leaving its pressure differential constant. From this point, increases in cathode liquid water content could divert flow though the bypass.

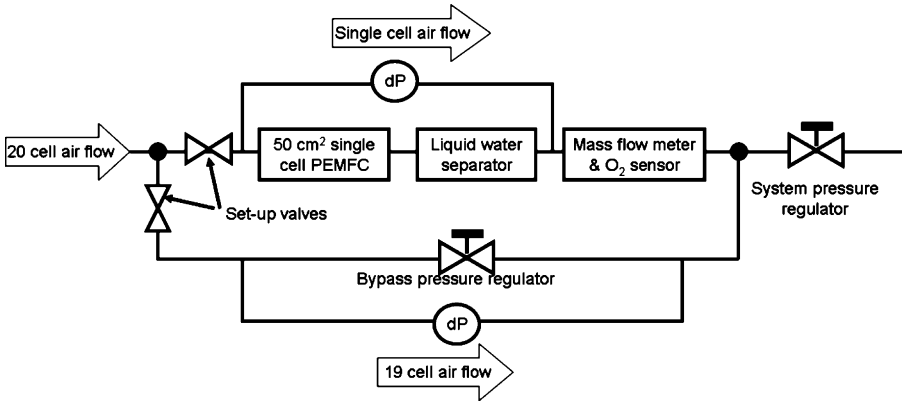

Fig. 2. Cathode bypass mechanization.

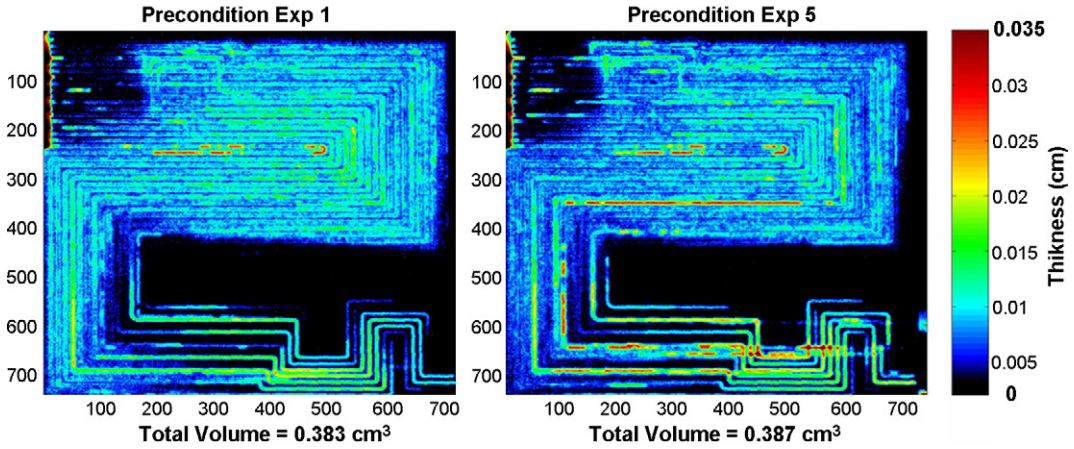

Fig. 3. Measurement repeatability demonstrated by comparison of same pre-condition run at beginning and end of the test protocol.

Once the cathode stoichiometric ratio fell below 1.0, the system was purged with high gas flow to remove liquid water and recover cell performance. After the purge, the cathode gas flow was returned to the beginning flow rate. Again, the cathode was allowed to slowly accumulate liquid water with its stoichiometric ratio proportionally decreased. This procedure was repeated several times with neutron imaging and purging both the cell and gas delivery system to remove all residual liquid water between experiments.

3. Results

Neutron images were acquired every 5.4 s during the experiment. This temporal resolution consists of a 2.0 s exposure and a 3.4 s file write time. Transient liquid water content and images were derived from an average of 10 individual images and steady state information consisted of 30 images averaged together. All fuel cell test stand parameters were recorded at a frequency of 1 Hz.

The precondition step previously described was run several times throughout the experiments, and a comparison of the steady-state liquid water accumulation allows one to consider the repeatability of the measurement. The liquid water distributions shown in Fig. 3 are representative of the precondition liquid water state of the test cell before the first and last experiments run in an extensive test protocol. The similarity shown here indicates a sufficient amount of time was allotted for the liquid water distribution to return to a consistent reference state.

Once a consistent reference saturation state was established, the cathode bypass loop was used to simulate stack cell-to-cell flow variations. Two test runs describing the liquid water accumulation in the cathode following the precondition are shown in Fig. 4. The data are aligned by the time ($t = 0$ s) at which the cell voltage approached zero, which is a cell failure due to lack of oxygen. For each experiment, the cell voltage, total liquid water volume (as measured via neutron radiography), and cathode stoichiometric ratio (as measured via the mass flow meter) are plotted as a function of time. As shown in Fig. 5, the cause of oxygen starvation at the point of cell failure is severe liquid water accumulation in the cathode flow distributor and gas diffusion media. The radiographs shown in Fig. 5 can be compared to the preconditions shown in Fig. 3. The additional liquid water accumulation in the cell is the cause of the rise in cathode flow field pressure differential which diverts increasing amounts of air into the bypass where the pressure differential is unchanged. In Fig. 4, the liquid water accumulation rate is observed to be proportional to the rate of stoichiometric ratio decrease in both experiments. In fact, for all experiments conducted under the same conditions using the cathode flow apparatus, this correspondence between liquid water accumulation and stoichiometric ratio was maintained regardless of the operational path taken to failure, or the initial condition.

For each experiment, the cell potential was recovered by purging with an increased flow rate of air after the cathode became flooded with liquid water. This was a successful recovery strategy as the purge instantly removed cathode channel slugs. As the purge continued, the liquid water content in the diffusion layer decreased slowly, indicating an evaporative removal mechanism. Moreover, this procedure indicated that GDL liquid water accumulation was not the primary contributor to the mass transport limitation leading to cell failure, as the cell potential recovered immediately after the channel slugs were removed. Once the cell

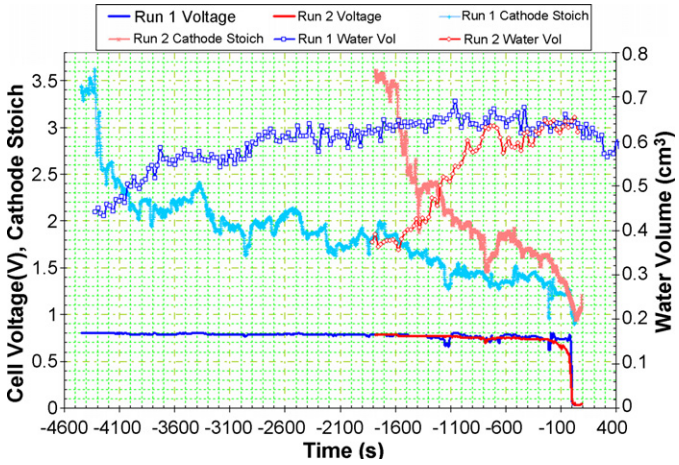

Fig. 4. Cell voltage response to cathode liquid water accumulation.

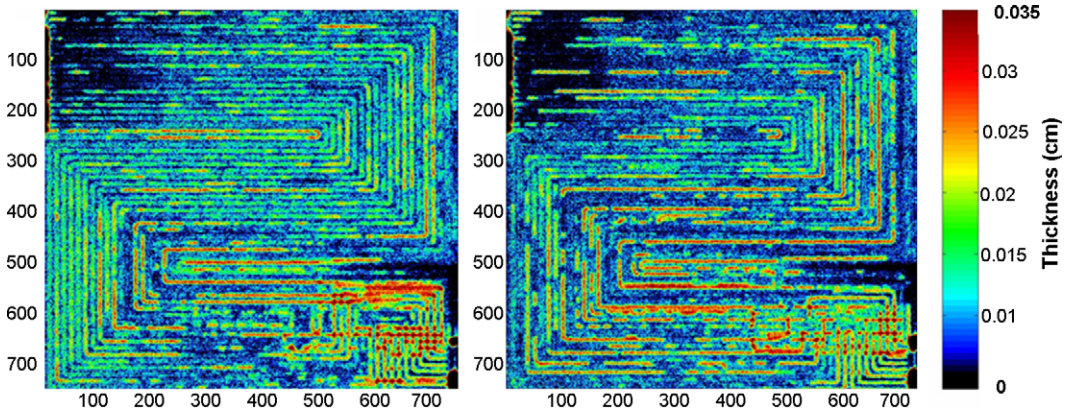

Fig. 5. Measured liquid water distribution at time of cell failure, corresponding to Runs 1 and 2 in Fig. 4.

returned to a relatively dry state, the cathode purge was stopped, returning to a bypassed flow configuration with an initial stoichiometric ratio of 3.4 at a current density of 0.2 A cm^{-2}. As shown in Fig. 6, for a repeat of the same experiment described in Fig. 4, from this point in the test protocol, liquid water build-up in the cathode flow distributor eventually caused an oxygen transport limitation and the cell potential approaches zero. The behavior shown in Fig. 6 is similar to that observed in Fig. 4, suggesting that the rate of accumulation or amount of liquid water at the oxygen transport limiting state is not history dependent. The liquid water distributions resulting from the cathode purge and at the point of cell potential loss is shown in Fig. 6.

Liquid water accumulation is found to occur in two modes. From an initial dry state (Fig. 6b), liquid water first accumulates in the gas diffusion layer and once the diffusion layer reaches a critical saturation fraction, the majority of liquid water is rejected into the channels in the form of droplets. It should also be noted that while water filling the channels is being measured, there is a small contribution from liquid water in the cathode inlet region of the GDL that is observed as the experiment progresses (Fig. 6b versus d). This is associated with the cathode inlet being initially dry as the relative humidity of the inlet gas (65%) is less than saturated. This allows for evaporation at the inlet. As the volumetric flow (stoichiometric ratio) decreases, the gas becomes

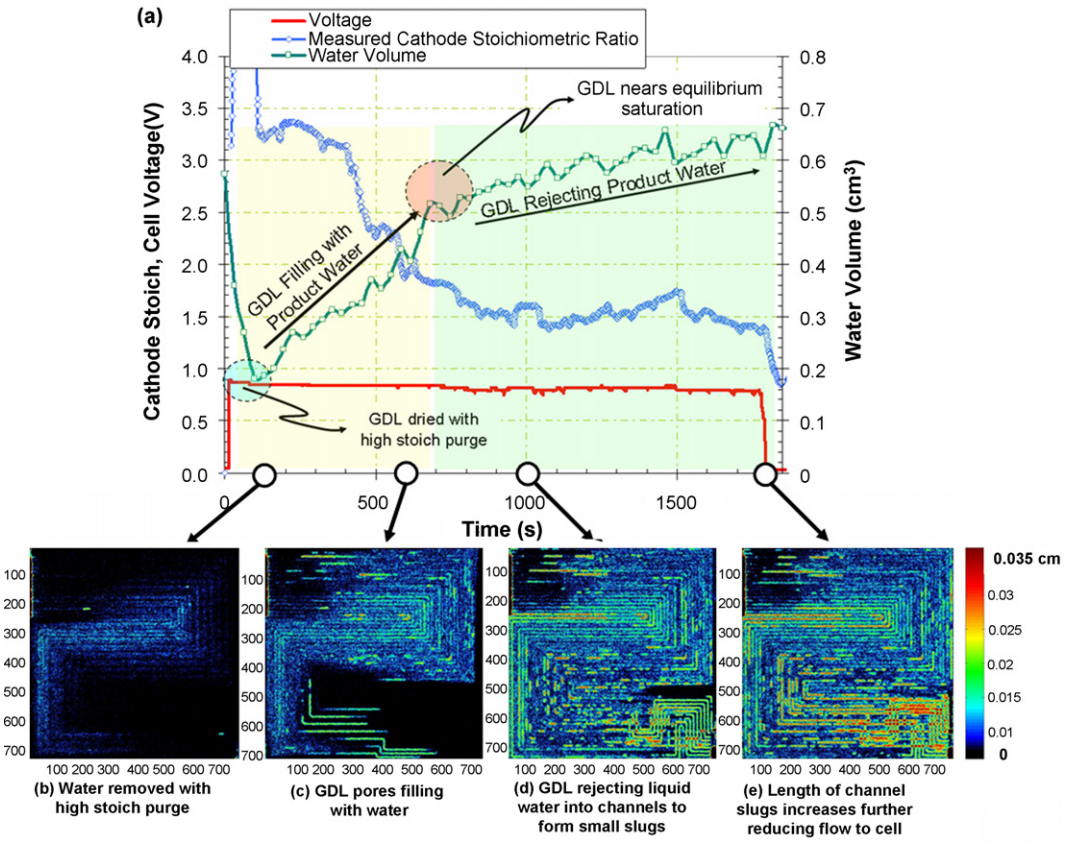

Fig. 6. Cathode response after liquid removed with purge.

saturated nearer to the inlet which results in GDL water at the inlet later in the experiment. Compared to the volume of water in the channels this contribution is very small.

In Fig. 6a, the two modes are distinguished by the change in slope of the time rate of change in measured liquid water volume. For the 50 cm^2 cell used in this experiment, at a current density of 0.2 A cm^{-2} water is generated at a rate of 0.93 mg s^{-1} [10], while the fastest rate of liquid water accumulation measured in all experiments was 0.50 mg s^{-1}, indicating that more than half the water produced is retained in the open volume of the GDL for a period of time after the onset of the experiment. From the results for three similar experiments presented in Figs. 4 and 6, it appears that there is a correlation between the rate of increase in the liquid water volume and the rate of decrease in the cathode stoichiometric ratio. The differences observed among experiments is due to the random behavior of slug formation and stagnation in the cathode flow channels for PEMFCs run under nominally identical conditions [1]. The liquid water content in the GDL is closely related to channel flow as higher flow has more capacity for evaporation and also provides convective flow though GDL to remove liquid water. Since the gas flow is very sensitive to small blockages in the system, this is thought to initiate the decline of cathode stoichiometric ratio.

To investigate further the relationship between liquid water volume and cathode stoichiometry, polynomials were fit to the data profiles shown in Fig. 6a such that the nonlinearity of the stoichiometric ratio decrease is preserved. These relationships are described as follows:

$$\text{liquid water volume}: \quad V_w = At + V_{w_o}, \tag{1}$$

$$\text{cathode stoichiometric ratio}: \quad \zeta_{air} = -Bt^2 - Ct + \zeta_{air_o}, \tag{2}$$

where A, B and C are constants.

These functions are approximations to the behavior observed in the initial GDL liquid water accumulation mode, as demonstrated in Fig. 7. This description of the measured cathode stoichiometric ratio and accumulated liquid water volume represents the particular data set reasonably well with correlation coefficients (R) of 0.935 and 0.955, respectively. The transition to the second accumulation mode is denoted by a sharp decrease in accumulation rate, as shown in Fig. 6. This transition results from the GDL reaching a critical saturation level, where for the given pore size distribution of the sample used and capillary pressure associated with the operating condition, no more GDL pores can be filled. At this condition, the unfilled pores will remain open and support gas transport. Once this critical saturation level has been reached all additional liquid water is rejected into the channels where it forms slugs that are intermittently removed, thus accounting for the second mode of accumulation where the rate is dependent on slug formation in the cathode channels (Fig. 6d).

Considering the first mode and how cathode flow conditions relate to liquid water accumulation one must discriminate the liquid water content in the anode GDL from the cathode. The two-dimensional neutron imaging technique that was used for these experiments lacks this information so individual anode and cathode gas purges were used to assess relative liquid water content by comparing the rate of liquid water removal during the purge. As shown in Fig. 8, from a reference state the anode stoichiometric ratio was increased from 2.0 to 9.5 then returned back to 2.0 and once the liquid water content reached the previous reference state the cathode stoichiometric ratio was increased from 2.0 to 4.0 (5.5 less than anode to maintain the same volumetric flow). The resulting change in liquid water content (Fig. 8) indicates that the majority of liquid water measured in the line integration through the fuel cell cross-section is located on the cathode side. The anode purge initially removes liquid water that was stagnant in the channels near the outlet and the remainder of the purge results in a slow removal of liquid water via evaporation of cathode water diffusing through the membrane. Water condenses near the outlet of anode channels due to consumption of hydrogen and this coupled with low outlet flow allows liquid water to stagnate. For the present work, anode channel water stagnation is considered to add on average 5% to the overall liquid water content measurements, and from the purge experiment results, the anode GDL is considered to have no liquid water content for the reported operating conditions.

In all experiments from the present study, the critical GDL saturation level (just before liquid water is rejected into channels) was reached at $(0.56 \pm 0.02)\,cm^3$ of liquid water volume ($V_{w,crit}$) in the system. If one subtracts the expected membrane

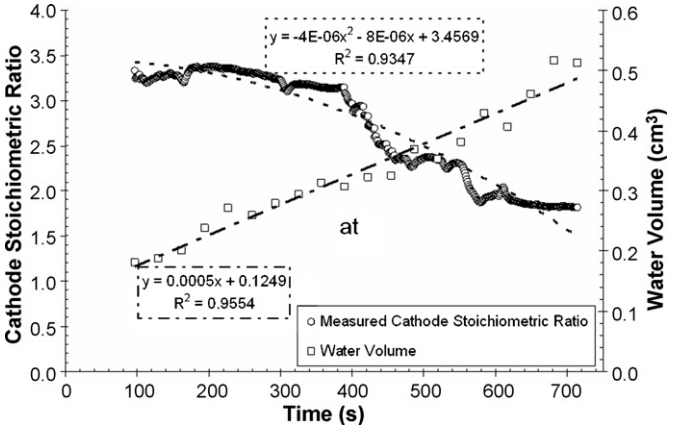

Fig. 7. Functional fit to measured data.

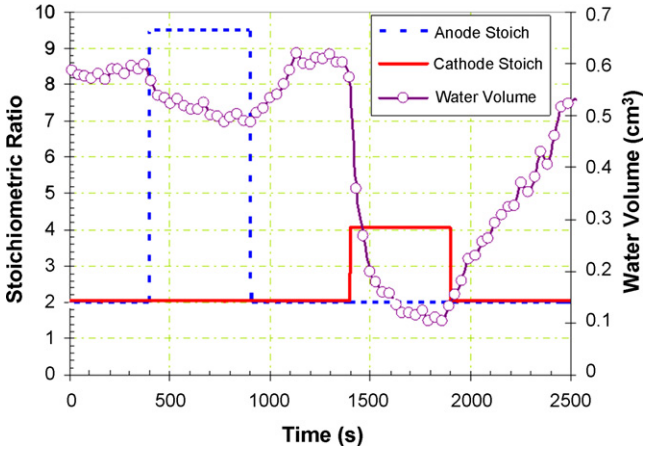

Fig. 8. Individual impact of anode and cathode gas purge on liquid water content within the cell.

Table 1
Eq. (3) constants fit with least squares regression to all experimental data

Constant	Value	Fit uncertainty
α	3.69	±0.13
β	173.5	±0.5
χ	−13.15	±0.02

water content [10], the critical saturation level is (35 ± 3)% of the open pore volume, based on the compressed thickness (210 μm) and porosity (80%) of the GDL. This saturation fraction correlates well to previous cathode GDL saturation fraction experiments [10].

Combining Eqs. (1) and (2) results in a relationship between cathode stoichiometric ratio (ζ_{air}) and liquid water volume (V_w) as the system approaches its critical saturation:

$$V_w = \alpha\left(\sqrt{(\zeta_{air_o} - \zeta_{air}) + \beta} + \chi\right) + V_{w_o}$$
$$\{\text{for } 0 < V_w < V_{GDL,crit}\}, \quad (3)$$

where α, β and χ are constants, and $V_{GDL,crit} = 0.35 V_{GDL,open}$.

Next the relationship described in Eq. (3) was applied to all experimental data including that shown in Fig. 4. With this functional relationship verified, the constants in Eq. (3) were fit with least squares regression to all experimental data, resulting in adjusted constants α, β and χ as reported in Table 1. The resulting correlation is shown in Fig. 9, where error is shown to be reduced to less than 20%.

This relationship is important because once the diffusion layer reaches a critical saturation level all liquid water is rejected into the channels where it begins to stagnate in the form of slugs. This second mode of accumulation will ultimately cause an oxygen limiting condition in one cell of many in a fuel cell stack. Initially these droplets leaving the GDL increase the pressure drop of the cell by reducing the channel cross-sectional area as the droplet forms. Without the flow required to detach the droplet from the GDL, some of the droplets continue to grow until they contact the adjacent channel wall and a slug is formed that blocks the entire channel cross-section. These slugs are found to form at sites throughout the cell and correspond to the active liquid water transport pore networks in the cathode GDL; see Fig. 6d.

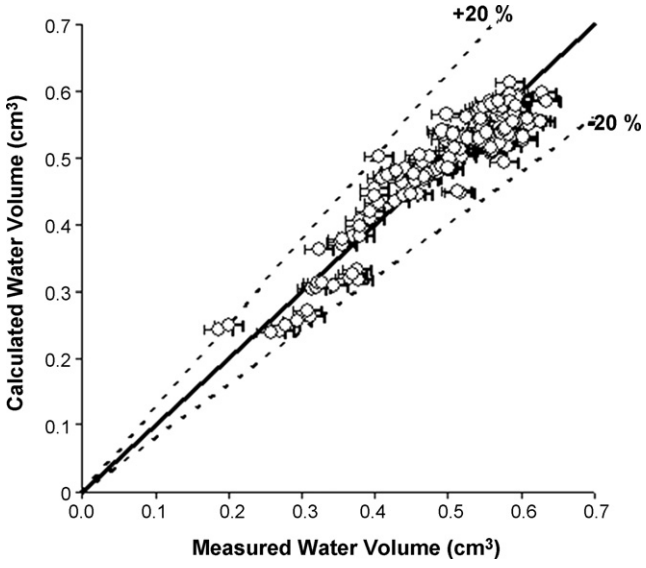

Fig. 9. Correlation of liquid water volume as a function of change in stoichiometric ratio with relationship fit to all experimental data.

Channel slugs are initially short and this allows air to bypass around the blockage in the channel through the GDL via the open gas transport pores. As time progresses, the active liquid water transport sites continue to reject liquid water which increases the length of the stagnant slugs (Fig. 6e). Since the in-plane pressure differential is a function of length through the GDL, this further restricts flow. This will ultimately cause the cathode stoichiometric ratio to fall below 1.0.

The average total liquid water volume for all experiments at the transport limiting point was 0.65 cm^3 and the calculated standard deviation was 0.01 cm^3. This consistently demonstrates that as the quantity of liquid water in the available cathode void volume (GDL pores and flow distributor channels) increases, the resulting rise in flow resistance redirects airflow away from the cell. As the cell receives less flow, the liquid water removed by convective and evaporative transport is reduced, leading to continued accumulation. Once a critical volume of liquid water has flooded the cathode GDL void volume, slug stagnation in the channels continues to restrict flow. The pressure rise at the inlet reduces the cathode stoichiometric ratio to below 1.0, and oxygen starvation impedes the reduction reaction. In all experiments, the cell potential reached an undesirable level (near 0 V) once about 18 of the 20 cathode flow channels developed a blockage somewhere along the length of the channel.

4. Conclusion

The cathode flow dynamics of a PEMFC stack were successfully simulated by a single fuel cell coupled with a flow bypass system. This arrangement allowed small increases in liquid water content and the associated pressure rise to divert flow through the bypass. The resulting liquid water accumulation was imaged and quantified with *in-situ* neutron radiography. The results consistently show that liquid water slugs blocking the cathode channels eventually divert enough flow to reduce the oxygen stoichiometric ratio below 1.0 and severe cell voltage loss results. The described mechanism could reduce performance in a stack, but is typically not captured with a single cell as these experiments do not allow increases in pressure differential to affect the stoichiometric ratio.

The time constant associated with the cathode flooding process is found to vary as the liquid water retention due to slug pinning in channels is somewhat unpredictable, but a direct correlation between stoichiometric ratio decrease and the rate of liquid water accumulation has been established. Moreover, the liquid water volume at the point of GDL saturation and the subsequent channel blockage resulting in voltage loss is found to be very repeatable. Results also show that the oxygen mass transport limitation and corresponding voltage loss is most sensitive to the cathode channel liquid water content, and liquid water accumulation in the diffusion layer has only an indirect influence. For the cathode flow channel design investigated, over

80% of the channels must be blocked with a liquid water slug somewhere along the channel length for oxygen starvation to occur.

Acknowledgements

This work was supported by the U.S. Department of Commerce, the NIST Ionizing Radiation Division, the Director's office of NIST, the NIST Center for Neutron Research, and the Department of Energy interagency agreement No. DE_AI01-01EE50660. The authors would also like to thank Lew DiPietro for his assistance with the experimental set-up.

References

[1] K. Tuber, D. Pocza, C. Hebling, J. Power Sources 124 (2003) 403–414.
[2] Q. Dong, J. Kull, M.M. Mench, J. Power Sources 139 (2005) 106–114.
[3] J. Stumper, M. Lohr, S. Hamada, J. Power Sources 143 (2003) 150–157.
[4] W. He, G. Lin, T.V. Nguyen, AIChE J. 49 (2003) 3221–3228.
[5] R. Satija, D.L. Jacobson, M. Arif, S.A. Werner, J. Power Sources 129 (2003) 238–245.
[6] A. Turhan, K. Heller, J.S. Brenizer, M.M. Mench, J. Power Sources 160 (2006) 1195–1209.
[7] J. Zhang, D. Kramer, R. Shimoi, Y. Ono, E. Lehmann, A. Wokaun, K. Shinohara, G.G. Scherer, Electochim. Acta 51 (2006) 2715–2727.
[8] M.A. Hickner, N.P. Siegel, K.S. Chen, D.N. McBrayer, D.S. Hussey, D.L. Jacobson, M. Arif, J. Electrochem. Soc. 153 (2006) A902–A908.
[9] T.A. Trabold, J.P. Owejan, D.L. Jacobson, M. Arif, P.R. Huffman, Int. J. Heat Mass Trans. 49 (2006) 4712–4720.
[10] J.P. Owejan, T.A. Trabold, D.L. Jacobson, D. Baker, D. Hussey, M. Arif, Int. J. Heat Mass Trans. 49 (2006) 4721–4731.
[11] P. Rodatz, F. Buchi, C. Onder, L. Guzzella, J. Power Sources 128 (2004) 208–217.
[12] P. Rapaport, Y. Lai, C. Ji, Proceedings of ASME Fuel Cell, 2006.
[13] D. Hussey, D.L. Jacobson, M. Arif, P.R. Huffman, R.E. Williams, J.C. Cook, Nucl. Instr. Phys. Res. A 542 (2005) 9–15.
[14] Certain trade names and company products are mentioned in the text or identified in an illustration in order to adequately specify the experimental procedure and equipment used. In no case does such identification imply recommendation or endorsement by the National Institute of Standards and Technology, nor does it imply that the products are necessarily the best available for the purpose.